Spontaneous emission in the waveguide free-electron laser

Avner Amir, Ilario Boscolo,* and Luis R. Elias
Quantum Institute, University of California, Santa Barbara, California 93106
(Received 1 April 1985)

The incoherent emission from an undulating electron beam in the presence of metallic boundaries is analyzed. A general method of solving Maxwell's equations is used to express the field of a single particle in terms of vector waveguide modes. It is shown that the radiation characteristics depend upon a parameter involving the energy, wiggler wavelength, and the waveguide transverse dimension. At some values of this parameter the energy spectrum and angular distribution will differ significantly from the analogous free-space results. The amount of energy emitted into resonator modes is also analyzed in terms of a similar expansion.

INTRODUCTION

In the free-electron laser (FEL) a relativistic electron-beam moves through a static periodic magnetic field (undulator). In a nonlasing operation, electromagnetic radiation is produced by the transversely accelerated particles. The amount and spectrum of this radiation, usually referred to as "incoherent" or "spontaneous," is a crucial factor in the start-up process of the FEL oscillator. Dynamical characteristics such as transverse emittance, energy spread, and angular deflection are well manifested in the spectrum and make it a useful diagnostic tool to investigate electron-beam trajectories.

The analysis of the radiation emitted by a wiggling particle was first discussed by Motz[1] using standard methods of classical electrodynamics. Similar calculations were made by Kincaid[2] and Colson[3,4] for helical and linear undulators. These articles discuss the polarization, frequency, and angular dependence of the emitted power. The related problems of emission from a tapered undulator and from misaligned trajectories have also been investigated.[5–7] The spontaneous emission has been measured experimentally in several FEL facilities.[6,8] The theoretical investigations mentioned above were all concerned with the electromagnetic radiation emitted in the absence of any boundaries, and they all used a well-known expression: the Fourier transform of the electromagnetic fields derived from the Lienard-Wiechert potentials.[9]

The need to use guiding structures in the FEL design (Fig. 1) arises when one wants to operate in the far-infrared and submillimeter wavelength region.[10] The large diffraction losses inherent in low Fresnel numbers imply the use of closed resonators rather than open ones. An additional restriction is the desire to keep a small gap between undulator plates in order to achieve large magnetic fields at the center. These considerations lead to a relatively flat and wide resonator for the University of California at Santa Barbara[10,11] (UCSB) FEL designed to operate at wavelengths near 400 μm. The spontaneous emission spectrum will be the subject of a forthcoming experiment in this facility.[12]

Emission of electromagnetic waves by undulating particles in the presence of metallic boundaries has been, however, a much less treated subject in the literature. Motz and Nakamura[13] gave a rather detailed discussion. Unfortunately, they considered an infinitely long wiggler in the calculation. As a consequence, the outcome did not possess a realistic bandwidth. In fact, the authors focused on the repeated interaction of the electrons with waves whose velocities are close to the electron velocity and whose amplitudes diverge for an infinite wiggler. We will discuss this phenomenon in a later section.

In a recent article by Haus and Islam,[14] an energy conservation argument is used to study the coupling of the electron beam to rectangular waveguide modes. It is shown that in the limit of a highly over-moded guide, a result similar to the free-space expression is reproduced. Indeed, by substituting mode wave-numbers for free-space directions, one obtains a complete analogy between the two cases in this limit.

Our work has been carried out independently of Ref.14 and concentrates on the differences rather than the similarities between the emission into the free and the bounded space. In the present article we apply a general method to analyze the radiation field of an undulating beam in the

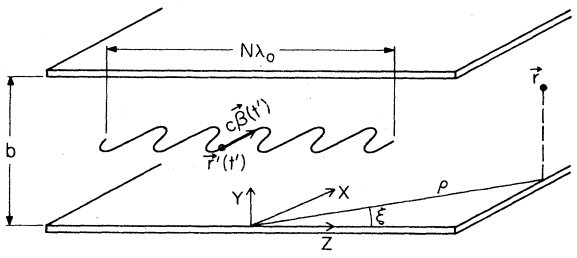

FIG. 1. The waveguide free-electron laser. Relativistic electrons move in a periodic fashion through a linear undulator (not shown) of length $N\lambda_0$. A single electron at point $\mathbf{r}'(t')$ moves with a velocity $c\boldsymbol{\beta}(t')$. The system is enclosed inside a waveguide (a set of two parallel conducting plates separated by a distance b). The radiation is observed at the point $\mathbf{r}$. A system of cylindrical (ρ,ξ,y) and of Cartesian (x,y,z) coordinates are shown.

presence of perfectly conducting boundaries. Maxwell's equations are combined to form a single inhomogeneous vector wave equation. This equation is solved by means of a matrix formalism known as the "dyadic Green's function."[15] The Green's-function method provides a convenient straightforward approach to complicated vector boundary-value problems.

The vector wave equation and the Green's-function method are introduced in Sec. I. In Sec. II, we show how this approach is used to derive the free-space-field spectrum normally obtained via the Lienard-Wiechert formula. This provides the branching point to the waveguide problem. In Sec. III, the method is applied to the case of a two parallel-plates waveguide. This configuration approximates the aforementioned flat rectangular waveguide currently in use at the UCSB FEL facility. The procedure, however, is very general and may be applied easily to waveguides of different geometry. The expressions obtained tend to be quite involved in the general case. In order to concentrate on the waveguide features and minimize the algebra, we introduce some obvious approximations associated with emission from a particle traveling in a weak magnetic field and suppress the higher harmonic content of the spectrum. This is unnecessary in general but allows us to focus on the important new aspects of the problem. The angular and frequency characteristics of the spectrum are discussed. It is shown that the emission line shape in a moderate-size waveguide is quite distinct from its free-space counterpart and may contain several maxima associated with the interference of the emission from the current and its "images." This results in a substantial power going into a small number of the waveguide modes. The number of the excited modes and their frequency spacing will be shown to be dependent on a parameter involving the energy, wiggler wavelength, and the transverse dimension of the waveguide. In the limit of a very large gap between the plates the spectrum resembles the free-space result. In this situation it is easy to draw the analogy between the power emitted into a unit solid angle in the free-space case and the power emitted into the corresponding phase-space element in our case.

Section IV is devoted to the resonator problem. The spontaneous emission power emitted into any of the modes of a resonator formed by introducing two cylindrical mirrors at the ends of the waveguide is evaluated here for the first time. Using this result we investigate the effect of the optical beam diffraction on the bandwidth of the emission line. Finally, we comment on the relation between the spontaneous and the stimulated emission in this particular case, a relation that is well known in the one-dimensional theory.[16]

Two appendices are added at the end. Appendix A introduces some notations used in the dyadic Green's-function formalism and some of its properties are summarized. Appendix B contains two different derivations of the relevant Green's function. The first is the standard one of eigenfunction expansion following the methods of Ref. 15. The second is a direct calculation based on the concept of image currents. This procedure is not applicable in general but provides a better insight into the problem.

I. THE VECTOR WAVE EQUATION AND ITS SOLUTION

In this section we discuss the formal solution of Maxwell's equation by means of the dyadic Green's function. Our starting point is the inhomogeneous Maxwell's equations in the absence of dielectric or permeable media (in cgs units):

$$\nabla\times\mathbf{B}-\frac{1}{c}\frac{\partial\mathbf{E}}{\partial t}=\frac{4\pi}{c}\mathbf{J}\,, \tag{1.1a}$$

$$\nabla\times\mathbf{E}+\frac{1}{c}\frac{\partial\mathbf{B}}{\partial t}=0\,. \tag{1.1b}$$

We define the Fourier transform and its inverse as

$$\mathbf{F}_\omega(\mathbf{r})=\int\mathbf{F}(\mathbf{r},t)e^{i\omega t}dt\,, \tag{1.2a}$$

$$\mathbf{F}(\mathbf{r},t)=\frac{1}{2\pi}\int\mathbf{F}_\omega(\mathbf{r})e^{-i\omega t}d\omega\,. \tag{1.2b}$$

Applying (1.2a) to the time-dependent quantities in (1.1) gives

$$\nabla\times\mathbf{B}_\omega+ik\mathbf{E}_\omega=\frac{4\pi}{c}\mathbf{J}_\omega\,, \tag{1.3a}$$

$$\nabla\times\mathbf{E}_\omega-ik\mathbf{B}_\omega=0\,, \tag{1.3b}$$

where $k=\omega/c$ is the free-space wave number. Combining Eqs. (1.3a) and (1.3b) results in the following vector wave equations:

$$\nabla\times\nabla\times\mathbf{E}_\omega-k^2\mathbf{E}_\omega=\frac{4\pi}{c}ik\mathbf{J}_\omega\,, \tag{1.4a}$$

$$\nabla\times\nabla\times\mathbf{B}_\omega-k^2\mathbf{B}_\omega=\frac{4\pi}{c}\nabla\times\mathbf{J}_\omega\,. \tag{1.4b}$$

With the appropriate choice of boundary conditions a solution for (1.4) may be written as[15,17]

$$\mathbf{E}_\omega(\mathbf{r})=i\frac{k}{c}\int\overleftrightarrow{G}_\omega(\mathbf{r},\mathbf{r}')\cdot\mathbf{J}_\omega(\mathbf{r}')d^3r' \tag{1.5}$$

and a similar one for $\mathbf{B}_\omega$ with an appropriate Green's function $\overleftrightarrow{G}$. $\overleftrightarrow{G}_\omega$ is a 3×3 matrix, the so-called dyadic Green's function. We will use dyadic notation throughout this work to represent matrix operations. Some information on dyads is given in Appendix A. A systematic presentation is to be found in Refs. 15, 17, and 18.

$\overleftrightarrow{G}_\omega$ satisfies the following matrix equation:

$$\nabla\times\nabla\times\overleftrightarrow{G}_\omega-k^2\overleftrightarrow{G}_\omega=-4\pi\overleftrightarrow{I}\delta(\mathbf{r}-\mathbf{r}') \tag{1.6}$$

and the appropriate condition at the boundaries depending on whether $\mathbf{E}$ or $\mathbf{B}$ is involved. The operation $\nabla\times\nabla$ on a dyad is explained in Appendix A. $\overleftrightarrow{I}$ is the idem factor or the identity matrix (the dyad $\hat{\mathbf{x}}\hat{\mathbf{x}}+\hat{\mathbf{y}}\hat{\mathbf{y}}+\hat{\mathbf{z}}\hat{\mathbf{z}}$). The advantage of using the vector equations (1.3) rather than the more conventional wave equations for vector and scalar potentials[19] lies in the relative simplicity in the construction of $\overleftrightarrow{G}_\omega$ for various boundary-value problems. It also eliminates the choice of any particular gauge in the solution since (1.5) relates the source directly to the field. A standard way to solve (1.6) is by means of an eigenfunction expansion similar to that used in scalar problems.

The eigenfunctions are the vector modes of the problem (in waveguides those may be the familiar TE, TM modes). They satisfy the homogeneous equation

$$\nabla\times\nabla\times\mathbf{E}_\omega-k^2\mathbf{E}_\omega=0 \tag{1.7}$$

and the given boundary condition. In certain problems, and in particular the free-space case, it is possible to follow a shortcut known as the Levine-Schwinger method.[20] By some simple manipulations it is easily found that, in the absence of boundaries $\overleftrightarrow{G}_\omega$ may be written as

$$\overleftrightarrow{G}_\omega(\mathbf{r},\mathbf{r}')=\left[\overleftrightarrow{I}-\frac{1}{k^2}\nabla\nabla'\right]g_\omega(\mathbf{r},\mathbf{r}') , \tag{1.8}$$

where g_ω is the solution of the scalar wave equation

$$(\nabla^2+k^2)g_\omega(\mathbf{r},\mathbf{r}')=-4\pi\delta(\mathbf{r}-\mathbf{r}') . \tag{1.9}$$

Solving (1.9) is of course a much easier task than dealing directly with (1.6).

II. THE FREE-SPACE PROBLEM

In this section we demonstrate how the formalism of Sec. I. leads to the expression commonly used to calculate the radiation power emitted by the FEL and other synchrotronlike devices in free space. In the absence of boundaries (1.9) possesses a solution in the form of spherical waves[9]

$$g_\omega(\mathbf{r},\mathbf{r}')=\frac{e^{ikR}}{R} , \tag{2.1}$$

where $R\equiv|\mathbf{r}-\mathbf{r}'|$. Substituting into (1.8) and performing the differentiation we obtain

$$\overleftrightarrow{G}_\omega(\mathbf{r},\mathbf{r}')=(\overleftrightarrow{I}-\mathbf{nn})\frac{e^{ikR}}{R}+O(R^{-2}), \tag{2.2}$$

where $\mathbf{n}=\mathbf{R}/R$. Terms of higher order than R^{-1} are neglected since they do not contribute to the radiation field. Combining (2.2) and (1.5) and using the definition in (1.2) it follows that

$$\mathbf{E}_\omega(\mathbf{r})=\frac{ik}{c}\int dt'\int d^3r'(\overleftrightarrow{I}-\mathbf{nn})\cdot\mathbf{J}(\mathbf{r}',t')\frac{e^{ikR+i\omega t'}}{R} . \tag{2.3}$$

Now consider the case of a single particle with charge e moving along a trajectory $\mathbf{r}'=\mathbf{r}'(t')$ with velocity $\boldsymbol{\beta}=\boldsymbol{\beta}(t')$. Its current density is

$$\mathbf{J}(\mathbf{r}',t')=ec\boldsymbol{\beta}(t')\delta[\mathbf{r}'-\mathbf{r}'(t')] . \tag{2.4}$$

Inserting (2.4) into (2.3) gives

$$\begin{aligned}\mathbf{E}_\omega(r')&=ike\int dt'[\boldsymbol{\beta}-\mathbf{n}(\mathbf{n}\cdot\boldsymbol{\beta})]\frac{e^{ikR+i\omega t'}}{R}\\&=-ike\int dt'[\mathbf{n}\times(\mathbf{n}\times\boldsymbol{\beta})]\frac{e^{ikR+i\omega t'}}{R} .\end{aligned} \tag{2.5}$$

We see that the significance of the $\overleftrightarrow{I}-(1/k^2)\nabla\nabla'$ operator is in picking up the current component transverse to the line of sight. The total energy emitted per unit frequency per unit solid angle is given by

$$\begin{aligned}\frac{d^2E}{d\omega d\Omega}&=2\frac{1}{2\pi}\frac{c}{4\pi}R^2|\mathbf{E}_\omega|^2\\&=\frac{c^2k^2e^2}{4\pi^2}\left|\int dt'[\mathbf{n}\times(\mathbf{n}\times\boldsymbol{\beta})]e^{i\omega t'+ikR}\right|^2 .\end{aligned} \tag{2.6}$$

The factor $2/2\pi$ is consistent with the definition (1.2) and with the assumption of equal contribution from negative and positive frequencies. An electron beam moving through the wiggler consists of many particles radiating in an incoherent fashion. The total emitted power, averaged over one light period, is obtained from (2.6) by multiplying it by the number of electrons flowing per unit time (I/e where I is the current).

Equation (2.6) is the well-known expression appearing in Ref. 9 where it has been derived by Fourier transforming the Lienard-Wiechert fields. Most of the calculations of radiation from synchrotronlike sources have been based on it. Evaluation of the integral for helical and linear wigglers are given in Refs. 2–4. We will briefly summarize the results below. Consider a particle moving along the axis of a planar wiggler; its motion, to leading orders of K/γ is described by the following equations:[4]

$$\beta_z=\beta_{z0}+\frac{1}{8}\left[\frac{K}{\gamma}\right]^2\cos(2k_0z') , \tag{2.7a}$$

$$\beta_x=-\left[\frac{K}{\gamma}\right]\cos(k_0z') , \tag{2.7b}$$

$$x'=-\frac{K}{k_0\gamma}\sin(k_0z') . \tag{2.7c}$$

$K=|e|B_0\lambda_0/2\pi mc$ is the magnet strength parameter, B_0 is the amplitude of the magnetic field, m is the electron rest mass, γ is the ratio of its energy to its rest mass, and $k_0=2\pi/\lambda_0$ where λ_0 is the undulator period. The center of motion of the particle is assumed to follow the wiggler axis. The implications of a finite dimension beam and other inhomogeneities are discussed elsewhere.[21]

The greatest contribution to the integral in (2.6) comes at frequencies where the phase of the integrand $\Phi=kR+\omega t-k_0z'$, is stationary, i.e., $\dot{\Phi}=0$. In the far field it follows that $\omega=\omega_0\beta_{z0}/(1-\beta_{z0}\cos\theta)$, where θ is the angle to the axis and β_{z0} is the initial axial velocity. This will be referred to as the *phase matching condition.* It requires that the phase of the emitted light in any direction will match that of the wiggling motion. Thus the spectrum contains a range of Doppler up-shifted frequencies decreasing with angle. The highest is obtained on axis $\omega(\theta=0)=2\gamma^2\omega_0$. The spectral width at a given direction is associated with the coherence time of the pulse and is found to be $\Delta\omega/\omega\approx1/N$ where N is the number of periods in the wiggler. For strong magnets, the electrons tend to complete more of their synchrotron orbits near the individual magnets and this results in a larger contribution into higher harmonics of $\omega_0/(1-\beta_{z0}\cos\theta)$. We will, however, restrict our discussion to small values of K, small enough to reduce the complicated sums of Bessel functions, appearing in the full expressions, to a concise form. It also enables us to make some shortcuts in the following derivation. Indeed, if one intends to keep the

lowest-order terms in powers of K and γ^{-1} only the following terms of Eq. (2.6) should be retained:

$$\frac{d^2E}{d\omega d\Omega}=\frac{c^2e^2k^2}{4\pi^2}\left[\left|\int dt' e^{i\omega t'-ik\mathbf{n}\cdot\mathbf{r}'}(\beta_x-n_x\beta_z)\right|^2 + \left|\int dt' e^{i\omega t'-ik\mathbf{n}\cdot\mathbf{r}'}n_y\beta_z\right|^2\right], \tag{2.8}$$

where the far-field assumption $R\approx r-\mathbf{n}\cdot\mathbf{r}'$ has been introduced. The terms proportional to β_z will lead to contributions of the same order of magnitude as the one with β_x, due to the off-axis travel of the charge, as given in (2.7c). They necessitate the introduction of off-diagonal elements of $\vec{\mathbf{G}}$ into the solution and make it difficult to write (1.4) as a set of uncoupled scalar equations for the field components.

The second term on the right-hand side of (2.7a) contributes mainly to higher harmonics and is negligible under our assumptions ($K,\gamma^{-1}\ll 1$). Introducing (2.7) into (2.8), expanding the exponentials to the lowest power of K (this replaces the standard harmonic expansion and agrees with it to the lowest order), and integrating over the time spent in the wiggler gives

$$\frac{d^2E}{d\omega d\Omega}=\frac{c^2e^2}{4\pi^2}\left[\frac{K}{\gamma}\right]^2\left[\frac{k}{k_0}\right]^2\left[\frac{\sin(\chi N\pi)}{\chi}\right]^2\left[\left[1-n_x{}^2\frac{k}{k_0}\right]^2+\left[n_xn_y\frac{k}{k_0}\right]^2\right], \tag{2.9}$$

where $\chi=[k-\beta_z(k\cos\theta+k_0)]/k_0$ and β_z is now used for β_{z0}. Equation (2.9) may be integrated over all angles to give the energy spectrum, or alternatively over all frequencies to give the angular spectrum. This is traditionally done by exchanging the function $\sin^2(\chi N\pi)/\pi^2$ with a δ function

$$\frac{\sin^2(\chi N\pi)}{\chi^2}\to N\pi^2\delta(\chi), \tag{2.10}$$

which is reasonable for large values of N. In the first case we get

$$\frac{dE}{d\omega}=\frac{e^2N\pi}{4\pi c}\left[\frac{K}{\gamma}\right]^2\left[\frac{k}{k_0}\right]\left[1+\left[\frac{k}{k_0\gamma^2}-1\right]^2\right]\times\Theta(2\gamma^2k_0-k) \tag{2.11}$$

where Θ is the unit step function

$$\Theta(u)=\begin{cases}1, & u\geq 0\\ 0, & u<0\end{cases}.$$

Equation (2.11) has been derived under the assumption of small angles but seems to provide a reasonable approximation over the whole range when compared with the numerical results in Ref. 14. The free-space spectrum shown in Figs. 2 and 3 has a sharp cutoff at a frequency that corresponds to emission on-axis. The power decreases toward the low-frequency end.

When integrating (2.9) over all the relevant frequencies and over the azimuthal angle ϕ one gets

$$\frac{dE}{d\cos\theta}=4\pi e^2K^2\gamma^4k_0N\frac{1+\gamma^4\theta^4}{(1+\gamma^2\theta^2)^5}. \tag{2.12}$$

This expression does not seem to have appeared elsewhere. A plot of this result is contained in Fig. 4. In what follows we will show that the situation depicted in Figs 2—4 may be altered significantly with the introduction of metallic boundaries.

When integrating (2.11) over all frequencies up to $2\omega_0\gamma^2$ we find the total energy emitted to be

$$E=\tfrac{2}{3}\pi e^2K^2\gamma^2k_0N. \tag{2.13}$$

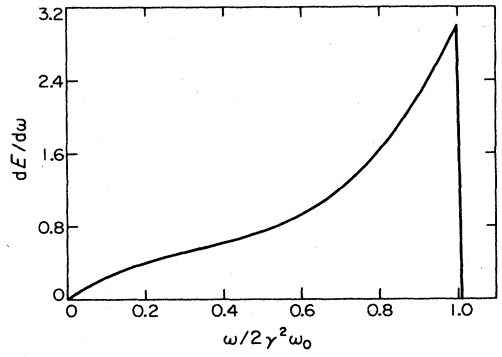

FIG. 2. The free-space spectrum. The frequency is normalized to its on-axis value $2\gamma^2\omega_0$. The energy per unit frequency interval is normalized to its average value: $E/2\gamma^2\omega_0=\pi e^2K^2N/3c$.

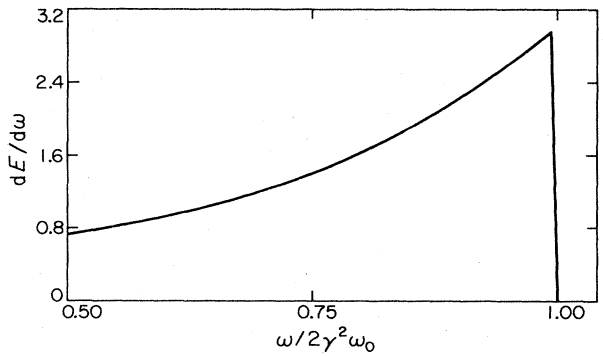

FIG. 3. The free-space spectrum in the range $\frac{1}{2}\leq\omega/2\gamma^2\omega_0\leq 1$ (this is to be compared with the results of Sec. III).

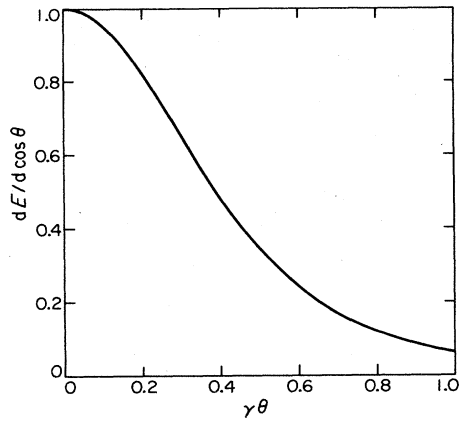

FIG. 4. Angular distribution at small angles. The quantity $dE/d\cos\theta$ is normalized to its on-axis value $4\pi e^2K^2\gamma^4k_0N$.

The total average power of a single particle is then

$$\langle P(t')\rangle=\frac{E}{N\lambda_0/c}=\tfrac{1}{3}e^2cK^2\gamma^2k_0^2\ . \tag{2.14}$$

This is exactly what one gets from the Lienard expression[9]

$$P(t)=\frac{2}{3}\frac{e^2}{c}\gamma^6[\dot{\boldsymbol{\beta}}^2-(\boldsymbol{\beta}\times\dot{\boldsymbol{\beta}}^2)]\ , \tag{2.15}$$

which is a simple relativistic generalization of the well-known Larmor formula.

III. THE RADIATION FIELD INSIDE A TWO PARALLEL-PLATES WAVEGUIDE

In this section we discuss the main subject of this paper which is the radiation field generated by an electron beam inside a waveguide. In the presence of metallic surfaces, electromagnetic waves may propagate provided they satisfy the spatial boundary conditions. As a result, a discrete set of wavelengths is allowed at any given frequency. This is the waveguide dispersion relation. From the free-space discussion, we know that there is a phase-matching condition for an effective particle-wave interaction. That condition will have to be modified by the dispersion relation. The result is the filtering out of those components that cannot interact effectively with the charge and propagate inside the guide at the same time.

Consider a particle undulating in the plane $y=b/2$ parallel to the plates of a two parallel-plates waveguide (Fig. 1). The plates are assumed to be perfect conductors and of infinite extent. The dyadic Green's function is essentially the field response to a unit current density flowing through a point $\mathbf{r}'=(x',y',z')$. The general expression for the Green's function is derived in Appendix B. It turns out, however, that in our case one may follow a route similar to the aforementioned Levine-Schwinger procedure, that is, derive the dyadic Green's function from the scalar one. This is also shown in detail in Appendix B. The scalar Green's function $g_\omega(\mathbf{r},\mathbf{r}')$ for this problem obeys the boundary conditions

$$g_\omega(y=0)=g_\omega(y=b)=0\ , \tag{3.1a}$$

$$g_\omega\to 0 \text{ as } \rho\to\infty\ , \tag{3.1b}$$

where $\rho=[(x-x')^2+(z-z')^2]^{1/2}$. By the method of separation of variables, one easily finds that a solution to (1.9) that satisfies (3.1) may be written as

$$g_\omega(\mathbf{r},\mathbf{r}')=\frac{2\pi i}{b}\sum_{m=1}^{\infty}H_0^{(1)}(k_{||}\rho)\sin\left[\frac{m\pi}{b}y\right]\sin\left[\frac{m\pi}{b}y'\right]\ , \tag{3.2}$$

where $H_0^{(1)}(k_{||}\rho)$ is the Hankel function of the first kind. It is a solution of the two-dimensional wave equation[18]

$$\left[\frac{\partial^2}{\partial x^2}+\frac{\partial^2}{\partial z^2}+k_{||}^2\right]H_0^{(1)}(k_{||}\rho)=0 \tag{3.3}$$

and may be considered the "unit wave" in two dimensions, analogous to (2.1). In the far field there is an asymptotic formula[18]

$$i\pi H_0^{(1)}(k_{||}\rho)\to(2\pi/k_{||}\rho)^{1/2}e^{ik_{||}\rho+i\pi/4} \tag{3.4}$$

so that (3.1b) is satisfied. Writing

$$\sin(m\pi y/b)\sin(m\pi y'/b)$$

as

$$\tfrac{1}{2}\,\mathrm{Re}(e^{im\pi(y-y')/b}-e^{-im\pi(y+y')/b})$$

and combining with (3.4) shows that in the far field, one may think about a mode as a pair of cylindrical waves (Fig. 5), originated at $\mathbf{r}'$ whose normals are given by the directions of

$$\mathbf{k}_\pm=(k_{||}\sin\xi,\pm m\pi/b,k_{||}\cos\xi)\ ,$$

where $k_{||}=(k^2-k_y^2)^{1/2}$, and ξ is the angle from the axis in the (x,z) plane such that $\rho=\rho(\sin\xi,0,\cos\xi)$. Following the steps through (2.5) we find that the field of a particle moving along a trajectory $\mathbf{r}'=\mathbf{r}'(t')$ with a velocity $c\boldsymbol{\beta}(t')$ is given by

$$\mathbf{E}_\omega(r')=ike\frac{2\pi i}{b}\sum_{m=1}^{\infty}\int dt'\left[\overleftrightarrow{\mathrm{I}}-\frac{1}{k^2}\nabla\nabla'\right]H_0^{(1)}(k_{||}\rho)\sin\left[\frac{m\pi}{b}y\right]\sin\left[\frac{m\pi}{b}y'\right]\boldsymbol{\beta}(t')e^{i\omega t'} \tag{3.5}$$

where an integration over $\mathbf{r}'$ has been carried out and all the primed coordinates became explicit functions of t'. The solution for the magnetic field is obtained from (1.3) and (3.5)

$$\mathbf{B}_\omega(\mathbf{r}')=-\frac{2\pi ie}{b}\sum_{m=1}^{\infty}\int dt'\nabla\times\left[\boldsymbol{\beta}(t')H_0^{(1)}(k_{||}\rho)\sin\left[\frac{m\pi}{b}y\right]\sin\left[\frac{m\pi}{b}y'\right]\right]e^{i\omega t'}\ . \tag{3.6}$$

The next thing would be to apply the operators in (3.5) and (3.6) which can be done without difficulty. In the far field, (3.4) may be used. It follows from the interpretation of g_ω given above that an angle of emission θ in free space can be associated with the pair of wave vectors $\mathbf{k}_\pm$ provided $\cos\theta=(k_{||}/k)\cos\xi$ (Fig. 5). The difference here is that only a discrete set of directions with respect to the y coordinate is allowed at a given frequency. Since the emission process itself is the same in both cases, one may expect, for a relativistic particle, that most of the radiation will go in shallow angles and so the relevant mode numbers fall within $m\pi/kb<\gamma^{-1}$. With this in mind, (3.5) and (3.6) simplify to

$$\mathbf{E}_\omega(\mathbf{r}')=ike\frac{2}{b}\sqrt{2\pi}e^{i\pi/4}\sum_m\int dt'\frac{e^{ik_{||}\rho}}{\sqrt{k_{||}\rho}}\left[\hat{\mathbf{x}}\left[\beta_x-\beta_z\frac{k_{||}}{k}\sin\xi\right]\sin\left[\frac{m\pi}{b}y\right]\right.$$
$$\left.+i\hat{\mathbf{y}}\frac{m\pi}{kb}\beta_z\cos\left[\frac{m\pi}{b}y\right]\right]\sin\left[\frac{m\pi}{b}y'\right]e^{i\omega t'}+O(\rho^{-3}/2\,,\,\gamma^{-2}\,,\,K^2)\,, \quad (3.7)$$

$$\mathbf{B}_\omega(\mathbf{r}')=-\frac{2ke}{b}\sqrt{2\pi}e^{i\pi/4}\sum_m\int dt'\frac{e^{ik_{||}\rho}}{\sqrt{k_{||}\rho}}\left\{\hat{\mathbf{x}}\frac{m\pi}{kb}\cos\left[\frac{m\pi}{b}y\right]+i\hat{\mathbf{y}}\left[\beta_x\sin\left[\frac{m\pi}{b}y\right]-\beta_z\frac{k_{||}}{k}\sin\xi\sin\left[\frac{m\pi}{b}y\right]\right]\right.$$
$$\left.-\hat{\mathbf{z}}\frac{m\pi}{kb}\cos\left[\frac{m\pi}{b}y\right]\sin\left[\frac{m\pi}{b}y'\right]\right\}e^{i\omega t'}+O(\rho^{-3/2}\,,\,\gamma^{-2}\,,\,K^2)\,. \quad (3.8)$$

Thus the particle couples mainly to TE modes. Next, let us calculate the total energy flowing into a unit area $dA=dx\,dy$ in the spectral range $(\omega,\omega+d\omega)$, in the direction $\hat{\boldsymbol{\rho}}=(\cos\xi,0,\sin\xi)$. It is given by the projection of the Poynting vector along this direction

$$\frac{d^2E}{d\omega dA}=2\frac{1}{2\pi}\frac{c}{4\pi}(\mathbf{E}_\omega\times\mathbf{B}_\omega^*)\cdot\hat{\boldsymbol{\rho}}\,. \quad (3.9)$$

Substituting (3.7) and (3.8) into (3.9) results in

$$\frac{d^2E}{d\omega dA}=\frac{2ck^2e^2}{\pi b^2}\left[\left|\sum_m\int\frac{e^{ik_{||}\rho+i\omega t'}}{\sqrt{k_{||}\rho}}\left[\beta_x-\beta_z\frac{k_{||}}{k}\sin\xi\right]\sin\left[\frac{m\pi}{b}y\right]\sin\left[\frac{m\pi}{b}y'\right]\right|^2\right.$$
$$\left.+\left|\sum_m\frac{m\pi}{kb}\int\frac{e^{ik_{||}\rho+i\omega t'}}{\sqrt{k_{||}\rho}}\beta_z\cos\left[\frac{m\pi}{b}y\right]\sin\left[\frac{m\pi}{b}y'\right]\right|^2\right]. \quad (3.10)$$

In the case of a particle traveling on axis ($y'=b/2$), only modes of even symmetry with respect to the center will contribute to the sum.

Let us now investigate the radiation detected over a slit of width Δx and length b located at the waveguide exit aperture (Fig. 6). Upon integrating (3.10) from 0 to b the cross-terms vanish and we get

$$\frac{d^2E}{d\omega dx}=\frac{ck^2e^2}{\pi b}\sum_{m\ \text{odd}}\left[\left|\int dt'\frac{e^{ik_{||}\rho+i\omega t'}}{\sqrt{k_{||}\rho}}\beta_x-\beta_z\frac{k_{||}}{k}\sin\xi\right|^2+\left|\int dt'\frac{e^{ik_{||}\rho+i\omega t'}}{\sqrt{k_{||}\rho}}\frac{m\pi}{kb}\beta_z\right|^2\right]. \quad (3.11)$$

If the slit and the detector are located at the far region with respect to the wiggler the integral in (3.11) may be evaluated. In other cases it must be done numerically. We found, however, that the characteristic shape of the spectrum is similar. Apparently, this shape is effected mainly by the phase matching condition and only slightly by the amplitude modulation that occurs at shorter distances. Using the far-field approximation we write

$$\rho\approx\rho_0-z'\cos\xi-x'\sin\xi, \quad (3.12)$$

where ξ is the angle to the center of the slit (Fig. 7) and ρ_0 is the distance to the center of the wiggler. Approximations such as (3.12) are implicit in all the free-space calculations.[1–5] Expanding the exponentials and keeping the resonant terms to the lowest order in K and γ^{-1}, Eq. (3.11) becomes

$$\frac{d^2E}{d\omega d\xi}=\frac{e^2}{\pi bc}\left[\frac{K}{\gamma}\right]^2\left[\frac{k}{k_0}\right]^2\sum_{m\ \text{odd}}\frac{1}{k_{||}}\left[\frac{\sin(\chi_m N\pi)}{\chi_m}\right]^2\left[\left[1-\frac{k_{||}^2}{kk_0}\sin^2\xi\right]^2+\left[\frac{k_yk_{||}}{kk_0}\sin\xi\right]^2\right], \quad (3.13)$$

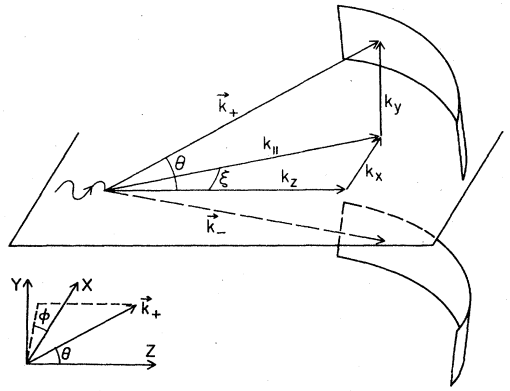

FIG. 5. Waveguide mode as a pair of cylindrical waves. In $\mathbf{k}$ space the wave vectors $\mathbf{k}_+,\mathbf{k}_-$ are perpendicular to the two phase fronts shown and are symmetric with respect to the central plane. $k_{||}$ is the projection on this plane. $k_y=m\pi/b$. The axial periodicity is given by $2\pi/k_z$.

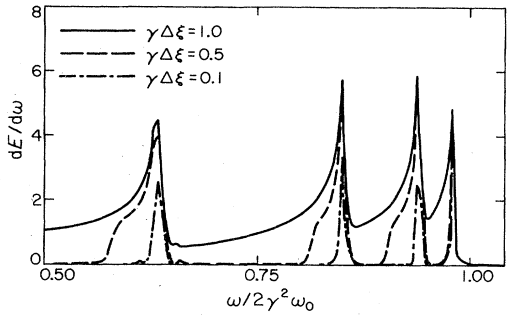

FIG. 7. Energy spectrum integrated over different slit widths: $\gamma\Delta\xi=0.1,0.5,1.0$. The lines broaden at the wider slit. The normalization is the same as in Fig. 2.

where $\chi_m=[k-\beta_z(k_{||}\cos\xi+k_0)]/k_0$ and $k_y\equiv m\pi/b$. Figure 7 shows the energy spectrum integrated over slits of different widths centered on axis. The spectrum contains some distinct maxima corresponding to the zeros of χ_m. The different spectral width of the lines is clearly associated with different angular acceptance in each case. Setting $\chi_m=0$ gives

$$k=\beta_z(k_{||}\cos\xi+k_0)\ . \tag{3.14}$$

Note that (3.14) is analogous to the free-space result

$$k=k_0/(1-\beta_z\cos\theta)\ .$$

The identification $\cos\theta=(k_{||}/k)\cos\xi$ follows directly from Fig. 5. Solving (3.14) for k we get

$$k=\beta_z\frac{k_0\pm[k_0^2-(1-\beta_z^2\cos^2\xi)(k_0^2+k_y^2\cos^2\xi)]^{1/2}}{1-\beta_z^2\cos^2\xi}$$
$$\approx\frac{k_0\gamma^2\pm\gamma[k_0^2\gamma^2-k_y^2(1+\gamma^2\xi^2)]^{1/2}}{1+\gamma^2\xi^2}\ , \tag{3.15}$$

where the last equation follows in the limit of small ξ. The "+" and "−" signs correspond to the Doppler up- and down-shifted frequencies, or photons emitted in the forward and backward directions, respectively, in the electron rest frame. (In a rectangular waveguide of dimensions a and b, Eqs. (3.14) and (3.15) are replaced by the following: (3.14) $k=\beta_z(k_{||}+k_0)$, (3.15) $k\approx\beta_z\{k_0\pm[k_0^2-\gamma^{-2}(k_0^2+k_x^2+k_y^2)]^{1/2}\}/(1-\beta_z^2)$, where k_x,k_y are the wave numbers associated with a,b.) We concentrate here on the up-shifted region. In the forward direction $\xi=0$, Eq. (3.15) reads

$$k(\xi=0)=\gamma^2[k_0+(k_0^2-\gamma^{-2}k_y^2)^{1/2}]\ . \tag{3.16}$$

There is a cutoff in frequencies when the quantity under the square-root sign vanishes. Imaginary values for $\mathbf{k}$ signify coupling to nonpropagating (evanescent) modes. Those modes are the counterpart of the neglected terms in Eq. (2.2). The cutoff occurs at $\mathbf{k}$ vectors forming an angle $\theta\approx k_y/k\approx k_0\gamma/(\gamma^2k_0)=1/\gamma$ with the z axis. The limit on the transverse mode index m is given by

$$m<2\gamma\frac{b}{\lambda_0}\ .$$

In fact, Eq. (3.15) may be derived directly and more meaningfully by using the concept of image currents com-

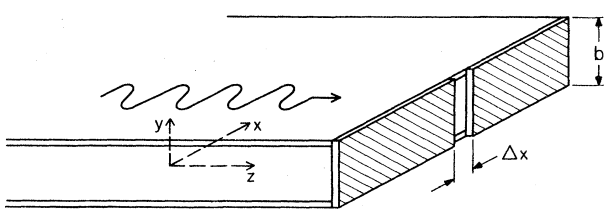

FIG. 6. A slit of width Δx at the end of the waveguide.

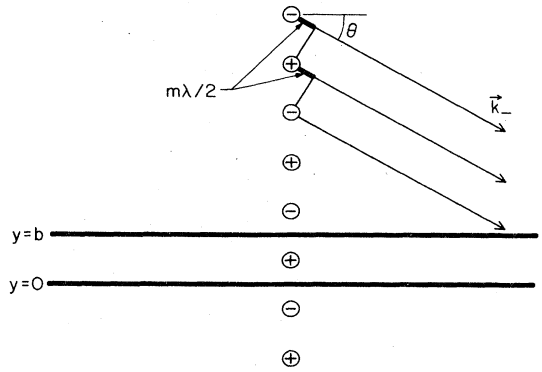

FIG. 8. A waveguide mode (only the half propagating in the $\mathbf{k}-$ direction is shown) will be driven most effectively by the set of equally spaced image charges provided they see alternating phases (the actual charge is located in the plane $y=b/2$).

bined with the free-space result. The image-currents construction is used in Appendix B as an alternative derivation for the Green's function. It consists of replacing the pair of plates with an infinite array of parallel currents of alternating signs (Fig. 8). All charges move in a similar fashion; each one emits the familiar wide-band free-space pattern. At far distances, a detector located on axis receives the interference pattern of the beam plus its images. A plane wave at an angle θ with respect to the axis will be driven most effectively by the set of charges provided that consecutive charges see phases which differ by π. The resulting condition is

$$\frac{m\lambda}{2}=b\sin\theta\ . \tag{3.17}$$

Combining (3.17) with the free-space frequency-angle dependence $k=k_0/(1-\beta_z\cos\theta)$ for a single particle leads to (3.16).

Equation (3.13) may also be integrated over the horizontal angle ξ to obtain the energy spectrum

$$\frac{dE}{d\omega}=\frac{e^2}{\pi bc}\left[\frac{K}{\gamma}\right]^2\left[\frac{k}{k_0}\right]^2\sum_{m\ \text{odd}}\frac{1}{k_{||}}\int d\xi\frac{\sin^2(\chi_m N\pi)}{\chi_m^2}\left[\left[1-\frac{k_{||}^2}{kk_0}\sin\xi\right]^2+\left[\frac{k_y k_{||}}{kk_0}\sin\xi\right]^2\right]. \tag{3.18}$$

The integration in Eq. (3.18) has been carried out numerically. Figures 9(a)–9(e) illustrate the change in the spectrum as the plates separation grows. The total number of excited modes increases with $\gamma b/\lambda_0$. The density of excited modes is higher at low indices as is evident from the figure. This corresponds to emission at shallow angles that "feels less" the effects of the walls. As the mode density grows, the lines tend to overlap and the characteristic slope of the free-space curve is reproduced, as will be shown shortly. The set of narrow peaks at moderate values of $\gamma b/\lambda_0$ is a manifestation of the constructive interference of the emission from the charge and its images that occurs when (3.14) is satisfied.

We may also integrate Eq. (3.13) over frequencies to find the angular distribution with respect to the angle ξ,

$$\frac{dE}{d\xi}=\frac{e^2}{\pi b}\left[\frac{K}{\gamma}\right]^2\sum_{m\ \text{odd}}\int dk\frac{1}{k_{||}}\left[\frac{k}{k_0}\right]^2\frac{\sin^2(\chi_m N\pi)}{\chi_m^2}\left[\left[1-\frac{k_{||}^2}{kk_0}\sin\xi\right]^2+\left[\frac{k_y k_{||}}{kk_0}\sin\xi\right]^2\right]. \tag{3.19}$$

Some plots of this result are shown in Figs. 10(a)–10(c). These graphs reveal another peculiar feature of emission in moderate size waveguides—the appearance of maxima located off axis. [In a rectangular waveguide energy can propagate only along the axis but similar phenomena still occur. Equation (3.21) is replaced by $(k^2-k_x^2-k_y^2)^{1/2}/k=\beta_z$. It is found that for a long wiggler significant power is carried by modes whose wave numbers k_x,k_y are not the smallest ones.] These maxima correspond to the excitation of photons moving in such directions that they can interact with the electron over prolonged periods of time. It is evident that the maxima disappear at shorter wiggler lengths. To investigate this analytically we may attempt to evaluate the k integral in (3.19) by replacing the function $\sin^2(\chi_m N\pi)/\chi_m^2$ with a δ function (considering the up-shifted branch only)

$$\frac{\sin^2(\chi_m N\pi)}{\chi_m^2}\to N\pi^2\delta(\chi_m)\to\frac{N\pi^2\delta(k-k^*)}{\left|1-\frac{k}{k_{||}}\beta_z\cos\xi\right|}\ , \tag{3.20}$$

where k^* is defined by $\chi_m(k^*)=0$. The denominator vanishes, and the integral in (3.19) becomes infinite when

$$\frac{k_{||}}{k}=\beta_z\cos\xi\ , \tag{3.21}$$

i.e., when the group velocity of the mode equals the component of the electron velocity in the direction of propagation. The infinity comes about because of the substitution (3.20) which amounts to the assumption of an infinite wiggler. In free space, the light always travels faster than the electrons and such situations cannot occur. Combining (3.21) with (3.14), we find that the peaks occur at angles $\xi_p=[(2b/m\lambda_0)^2-\gamma^{-2}]^{1/2}$. Small ξ_p requires large index m and vice versa. In either case a mode made of such photons will suffer considerable losses (conductive or diffractive) compared to modes consisting mainly of on-axis photons and it seems unlikely that it will reach the oscillation phase in a conventionally designed resonator.

Next, let us calculate the total energy radiated in the over-moded (the limit of large b) case. In a large size waveguide, the density of modes is larger and one may replace the sum in (3.18) by an integral

$$\frac{\pi}{b}\sum_{m\ \text{odd}}f\left[m\frac{\pi}{b}\right]\to\tfrac{1}{2}\int f(k_y)dk_y\ , \tag{3.22}$$

where the factor $\frac{1}{2}$ comes from the selection of odd modes only. In this case the total radiated energy is

$$E=\frac{e^2}{\pi^2}\left[\frac{K}{\gamma}\right]^2\frac{1}{k_0^2}\int\int\int dk_y d\xi\, dk\frac{k}{k_{||}}\frac{\sin^2[\chi(k_y)N\pi]}{[\chi(k_y)]^2}\left[\left[1-\frac{k_{||}^2}{kk_0}\sin^2\xi\right]^2+\left[k_y\frac{k_{||}}{kk_0}\sin\xi\right]^2\right]. \tag{3.23}$$

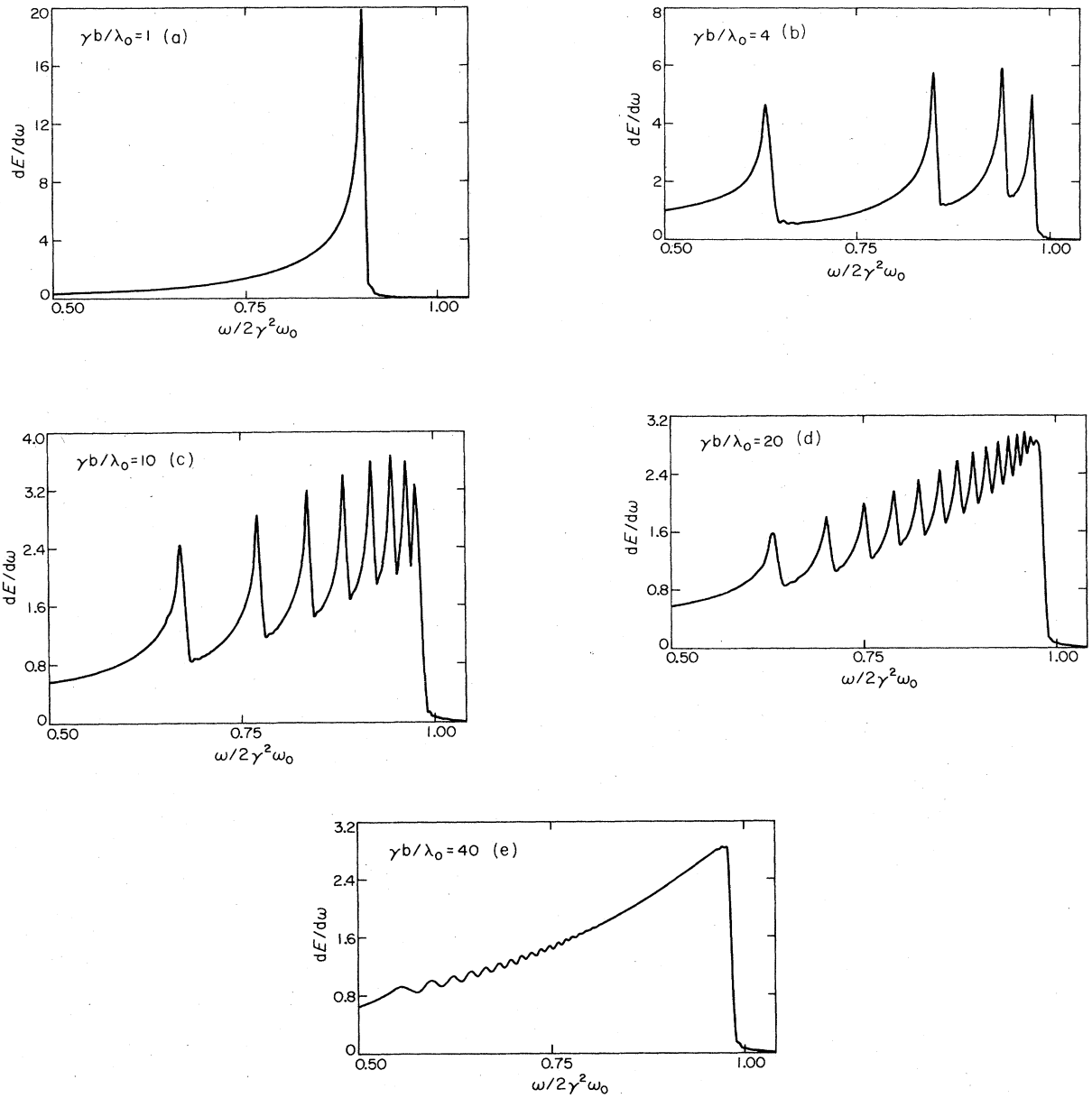

FIG. 9. (a)—(e) The waveguide energy spectrum for different values of $\gamma b/\lambda_0$. Note that the density of the excited modes is larger at low indices (the lowest index corresponds to the smallest angle of emission). (e) should be compared with Fig. 3. [The UCSB FEL parameters are those in (b).]

The physical description of the modes as a pair of cylindrical waves suggests the following change of variables:

$$k_{||}\cos\xi = k\cos\theta\ ,$$

$$k_y = k\sin\theta\sin\phi\ ,$$

from which we get $dk_y d\xi = k\, d\cos\theta\, d\phi$. Equation (3.23) becomes

$$E=\frac{e^2}{4\pi^2}\left[\frac{K}{\gamma}\right]^2\frac{1}{k_0^2}\int\int\int d\phi\, d\cos\theta\, dk\frac{\sin^2[\chi(k_y)N\pi]}{[\chi(k_y)]^2}\left\{\left[1-n_x^2\left[\frac{k}{k_0}\right]\right]^2+\left[n_x\frac{k_{||}}{k_0}\right]^2\right\}, \tag{3.24}$$

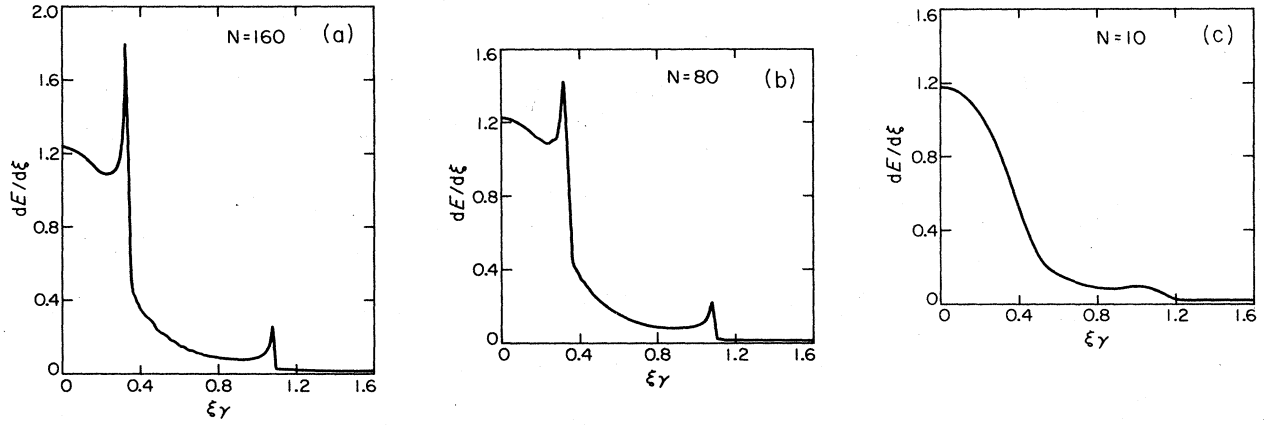

FIG. 10. The angular distribution of the radiation shows peaks at angles where the modes travel in group velocities comparable to the electron velocity. This behavior disappears at shorter wigglers. (a) $N=160$, (b) $N=80$, (c) $N=10$. The normalization is the same as in Fig. 4.

where the assumption of small angles has been used to make $k/k_{||}\approx 1$ and another factor of $\frac{1}{2}$ is inserted on account of the fact that $k_y \geq 0$. Equation (3.24) is identical to the integral of (2.8) and we conclude that

$$E_{(\text{over moded})}=\tfrac{2}{3}\pi e^2K^2\gamma^2k_0N\ . \tag{3.25}$$

We have actually shown that the same energy goes into similar phase-space elements. Equation (3.25) is in agreement with the common intuition that the effect of the walls in the over-moded case is just to reflect the incident waves and the total power stays the same. In the opposite case which is of a very small size waveguide, this fact is no longer true. It is clear that as we decrease the waveguide dimension the cutoff frequency increases and at $b=\lambda_0/2\gamma$ all the frequencies in (3.17) become complex; in other words, the electron excites only evanescent modes. In intermediate cases we found numerically that a large portion of the energy in (3.25), though not all, is coupled to propagating modes. This fraction oscillates around a number that grows with the waveguide size.

IV. THE EXCITATION OF RESONATOR MODES

In this section we analyze the amount of power that goes to each of the possible resonator modes. The resonator is formed by placing two wide cylindrical mirrors at the ends of the waveguide.[11] The resulting set of modes allows the energy to propagate in only a limited range of angles in the horizontal (x,z) plane. This in turn is translated into a limited range of frequencies appearing in the spectrum in much the same way as illustrated in Fig. 7. The empty cavity modes have been discussed before.[10] Such modes possess a trigonometric variation in the narrow dimension and the familiar Hermite-Gaussian[22] structure in the wide dimension. They are given by

$$\Psi_{mn}(\mathbf{r})=\sin\left[\frac{m\pi}{b}y\right]g_n(k_{||},x,z)\ , \tag{4.1}$$

where

$$g_n(k_{||},x,z)=\left[\frac{w_0}{w(z)}\right]^{1/2}H_n\left[\frac{x\sqrt{2}}{w(z)}\right]\exp[-x^2/w(z)^2+ik_{||}x^2/2R(z)-i(n+\tfrac{1}{2})\tan^{-1}z/z_0+ik_{||}z]\ .$$

H_n are the Hermite polynomials, w_0 is the beam waist, $z_0=\frac{1}{2}k_{||}w_0^2$ is known as the "Rayleigh length," $w(z)=w_0(1+z^2/z_0^2)^{1/2}$ and $R(z)=z+z_0^2/z$ is the radius of curvature of the wavefront. In order for these modes to satisfy the longitudinal boundary condition, the round-trip phase between mirrors must be an integer number of 2π. This implies some discrete values for k given by

$$k_{m,n,p}^2=\left[\frac{m\pi}{b}\right]^2+\left[\frac{\pi}{l}\left[p+\frac{n+\frac{1}{2}}{\pi}\cos^{-1}(s_1s_2)^{1/2}\right]\right]^2\ ,$$

where p is an integer, the *longitudinal index* of the mode, l is the resonator length, and $s_i=1-l/R_i$ where R_1,R_2 are the mirrors radii of curvature. The axial mode spacing is, however, normally two to three orders of magnitude smaller than the transverse mode spacing and will be suppressed in the following considerations.

It can be shown[23] that our scalar Green's function (3.2) may be expanded in terms of such modes upon using the asymptotic expression (3.4) and the Fresnel's approximation

$$\rho \approx z - z' + \frac{1}{2}\frac{(x-x')^2}{z-z'} . \tag{4.2}$$

The result is

$$g_\omega(\mathbf{r},\mathbf{r}') = \frac{4\pi i}{b\omega_0}\sum_{m,n}\frac{1}{k_{||}}\frac{1}{2^n n!\sqrt{\pi/2}}\Psi_{m,n}(\mathbf{r})\Psi^*_{mn}(\mathbf{r}') . \tag{4.3}$$

In doing so, we have uncoupled the coordinates $\mathbf{r},\mathbf{r}'$ and an expansion of the form

$$\mathbf{E}(\mathbf{r}) = \sum_{m,n}\mathbf{A}_{mn}\Psi_{mn}(\mathbf{r})$$

may easily be written. [It is worth mentioning that in the more commonly used open resonator (with circular symmetry around the axis), one can obtain a similar expansion. The approximation (4.2) has an extra term then which yields another two factors in (4.3) containing the y,y' coordinates.] Such an expression would be rather difficult to get directly from the wave equation under the assumptions of the paraxial approximation. [In the common method of deriving the paraxial wave equation[22] one usually looks for a transversely polarized solution, thereby obtaining a single scalar wave equation for the transverse field. This assumption is inappropriate here in light of the discussion following Eq. (2.8). For a systematic way of treating the paraxial approximation see Ref. 24.] We now proceed along similar steps as those leading from (3.10) to (3.18). As before, it is easy to see that to lowest order in K and γ^{-1} the relevant terms in the operator $\overleftrightarrow{\mathbf{I}} - (1/k^2)\nabla\nabla'$ are

$$\hat{\mathbf{x}}\hat{\mathbf{x}} - \hat{\mathbf{y}}\hat{\mathbf{z}}\partial_y\partial_{z'}/k^2 - \hat{\mathbf{x}}\hat{\mathbf{z}}\partial_x\partial_{z'}/k^2 .$$

Starting from

$$\mathbf{E}_\omega(\mathbf{r}) = -4\pi k\frac{e}{bw_0}\sum_{m,n}\frac{1}{k_{||}}\frac{1}{2^n n!\sqrt{\pi/2}} \times \int dt' \left[\hat{\mathbf{x}}\hat{\mathbf{x}} + i\hat{\mathbf{y}}\hat{\mathbf{z}}k_{||}\frac{\partial_y}{k^2} + i\hat{\mathbf{x}}\hat{\mathbf{z}}k_{||}\frac{\partial_x}{k^2}\right] g_m(k_{||},x,z)g_n^*(k_{||},x',z')\sin\left[\frac{m\pi}{b}y\right]\sin\left[\frac{m\pi}{b}y'\right]\beta(t')e^{i\omega t'} \tag{4.4}$$

and carrying out the derivatives, the fields may be found and are given conveniently by a linear expansion in terms of the modes. After some more algebra the total energy per unit frequency is found to be

$$\frac{dE}{d\omega} = \frac{2\pi^2e^2}{cbw_0}\left[\frac{K}{\gamma}\right]^2\left[\frac{k}{k_0}\right]^2\sum_{n,m\ \text{odd}}\frac{1}{k_{||}^2}\left[\left|\left[1-\frac{2k_{||}}{k^2k_0w_0^2}(n+1)^2\right]A_n - \frac{2k_{||}}{k^2k_0w_0^2}(n-1)A_{n-2}\right|^2 + \left|\frac{k_yk_{||}}{k^2k_0}\frac{\sqrt{2}}{w_0}2nA_{n-1}\right|^2\right] , \tag{4.5}$$

where the recursive relations for the Hermite polynomials and

$$\frac{\partial}{\partial x}g_n(k_{||},x,z) = \frac{\sqrt{2}}{w_0}[n g_{n-1}(k_{||},x,z) - \tfrac{1}{2}g_{n+1}(k_{||},x,z)]$$

have been used. For the definition of A_n we use the notations[25] $q = \beta_z L/z_0, \tau = ct'/L$. It is given by

$$A_n = \frac{H_n(0)}{(2^n n!\sqrt{\pi/2})^{1/2}}\int_{-1/2}^{1/2}d\tau\frac{1}{(1+q^2\tau^2)^{1/4}}\exp[2\pi i\chi N\tau + i(n+\tfrac{1}{2})\tan^{-1}(q\tau)] \tag{4.6}$$

and $A_n = 0$ for $n < 0$ by definition. Here $\chi = [k - \beta_z(k_0 + k_{||})]/k_0$. Let us investigate the limit of small q (large z_0 is the limit of small diffraction). Equation (4.6) reduces to

$$|A_n| \to \frac{H_n(0)}{(2^n n!\sqrt{\pi/2})^{1/2}}\frac{\sin[\chi N\pi + \frac{1}{2}q(n+\frac{1}{2})]}{[\chi N\pi + \frac{1}{2}q(n+\frac{1}{2})]} . \tag{4.7}$$

This leads to a new phase-matching condition

$$k - \beta_z(k + k_{||}) + \frac{2\beta_z(n+\frac{1}{2})}{k_{||}w_0^2} = 0 .$$

We note that the new condition amounts to an effective new wavelength $k_{||} \to k_{||}[1-(2n+1)/k_{||}^2w_0^2] \approx [k^2 - (m\pi/b)^2 - (4n+2)/w_0^2]^{1/2}$. The Hermite-Gaussian mode, which is a combination of photons spread over a characteristic angle $\xi \approx (4n+2)^{1/2}/k_{||}w_0$, is thus best excited in this limit at a center frequency given approximately by an expression similar to (3.15),

$$k \approx \beta_z\gamma^2(k_0 + \{\beta_z^2k_0^2 - [(m\pi/b)^2 + 4(n+\tfrac{1}{2})/w_0^2]\gamma^{-2}\}^{1/2}) . \tag{4.8}$$

This is slightly different from the one required to excite on-axis ($\xi=0$) photons.

Finally, let us find the amount of energy flowing into the fundamental Gaussian mode. It is given by

$$\left[\frac{dE}{d\omega}\right]_{n=0}=\frac{2\pi^2e^2N^2}{cbw_0}\left[\frac{K}{\gamma}\right]^2\left[\frac{k}{k_0}\right]^2\sum_{m\ \text{odd}}\frac{1}{k_{||}^2}\left[1-\frac{2k_{||}}{k^2k_0w_0^2}\right]^2|A_0|^2. \tag{4.9}$$

In the case of a general q it is not possible to write an expression like (4.8). In Fig. 11, several plots of $\sqrt{q}\,|A_0|^2(\propto|A_0|^2w_0^{-1})$ as a function of q are shown for $m=1$. The broadening of the peak and its height vary with q due to different angular spread and average on-axis intensity in each case. A beam of a wider angular spread introduces more low-frequency components into the spectrum which results in shifting the maximum to the left. [This dependence of the center frequency on q is also evident in (4.8) since $q\propto 1/w_0^2$.] We see that there is a maximum near $q=7$ from which one can figure out the optimum beam waist for a given electron energy and wiggler length. Figure 12 shows the spectrum of the energy in the fundamental and the $n=2$ Gaussian mode, for a typical value, $q=5$. We note the shift of the centers of the lines due to different angular patterns of the modes. A larger transverse spread in a normalized mode also implies smaller average intensity on axis which reduces the amount of excitation at higher indices.

Finally, the results of this section when combined with those of an earlier work[26] seem to indicate that the relation between spontaneous and stimulated emission for the particle-wave interaction known as "Madey theorem"[16] may hold, at least approximately, in our three-dimensional case. The only complication arises from the contribution of nontransverse components of the charge velocity [which resulted, for example, in the second term inside the last set of parentheses in Eq. (4.9)]. This relation will be investigated further in a forthcoming paper.

CONCLUSION

The dyadic Green's-function approach has been shown to provide a convenient and methodical way for dealing with the vector character of our problem.

The spectral and angular characteristics of the radiation emitted in free space and in a waveguide have been calculated and compared. We found that for large values of the parameter $\gamma b/\lambda_0$ the presence of the walls does not affect the spectral distribution but simply redirects the emitted light. At moderate values, interference effects occur which tend to change the appearance of the spectrum into a small number of relatively narrow lines. Each line corresponds roughly to the excitation of single waveguide mode.

The angular distribution shows that some significant power may be associated with modes containing photons that travel at large off-axis angles. These modes will suffer significant losses and are not expected to enter the lasing phase.

A similar analysis was done in terms of resonator modes. The spectrum of those was shown to be largely influenced by their angular spread and the average on-axis intensity.

The present analysis provides information that can be used to assess the three-dimensional evolution of the FEL oscillator. Such a theory (in the form of a set of rate equations for the modes coefficients) must include also a realistic mechanism for gain and losses in the different modes.

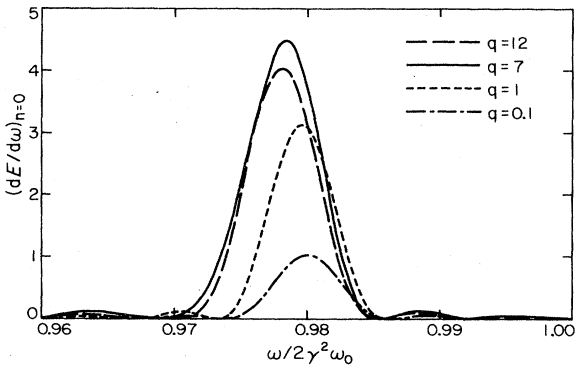

FIG. 11. Energy spectrum in the fundamental ($n=0,m=1$) sine-Gaussian mode. $|A_0|^2q^{1/2}$ is plotted at different values of the parameter q. The variations in the width and heights of the peaks are due to different angular spread and average on-axis intensity in the different cases. As q gets smaller the beam looks more like a plane wave and the spectrum tends to have the "homogeneous" bandwidth $1/N$.

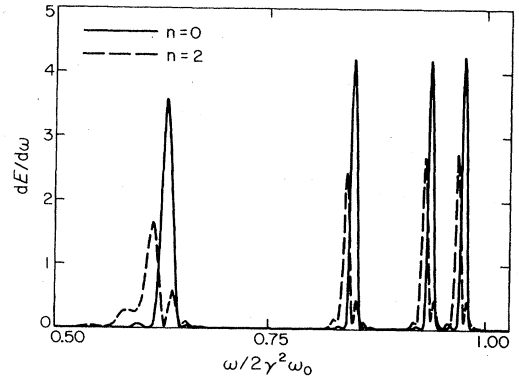

FIG. 12. Energy spectrum at different Hermite-Gaussian modes ($n=0,2,m=1,3,5,7$). Only the first term (proportional to A_n) in Eq. (4.5) is significant for the parameters chosen. Each "horizontal" mode contains the contribution of four "vertical" modes. [Four different values of m contribute to the sum in Eq. (4.9).] Note that for the $n=2$ mode the curve shifts and the peaks are smaller and broader. This is due to different angular spread and on-axis intensity of the two Gaussian modes. (In this case $\gamma b/\lambda_0=4$, $q=5$.)

ACKNOWLEDGMENTS

We are grateful for many helpful comments from W. B. Colson, Y. Greenzweig, and J. Gallardo. This work was supported by the U.S. Office of Naval Research (ONR) of the Department of the Navy and the U.S. Air Force Office for Scientific Research of the Department of the Air Force under ONR Contract No. N00014-80-C-308.

APPENDIX A: DYADS

In this appendix we summarize some properties of dyads. This is done merely to introduce the notation used in this paper. More detailed information may be found in Refs. 15, 17, and 18.

A *dyad* is simply a pair of vectors written in a definite order. From the vectors **a** and **b** we can form the dyad **ab**. The dyad **ab** is equivalent to a 3×3 matrix whose elements are formed by the outer product of the two vectors.

Having written a matrix in this way, the transformation of a vector may be defined in terms of vector operations only. Thus the result of the transformation **ab** on a vector **c** written on either side of the dyad may be defined in terms of the scalar products with the corresponding vectors

$$\mathbf{ab}\cdot\mathbf{c}=\mathbf{a}(\mathbf{b}\cdot\mathbf{c}) , \tag{A1a}$$

$$\mathbf{c}\cdot\mathbf{ab}=(\mathbf{c}\cdot\mathbf{a})\mathbf{b} . \tag{A1b}$$

The result of this operation is a vector. In a similar fashion, we may define the cross-product between a dyad and a vector. The result of this operation is a dyad

$$\mathbf{ab}\times\mathbf{c}=\mathbf{a}(\mathbf{b}\times\mathbf{c}) , \tag{A2a}$$

$$\mathbf{c}\times\mathbf{ab}=(\mathbf{c}\times\mathbf{a})\mathbf{b} . \tag{A2b}$$

In (A1b) and (A2b) we may replace the vector **c** with ∇ operator. Thus

$$\nabla\times(\mathbf{ab})=(\nabla\times\mathbf{a})\mathbf{b} . \tag{A3}$$

This notation appears in Eq. (1.6).

A *dyadic* $\overleftrightarrow{G}$ is a linear combination of dyads

$$\overleftrightarrow{G}=\sum_i a_i\mathbf{f}_i\mathbf{h}_i . \tag{A4}$$

In the solutions of various linear inhomogeneous vector equations the relation between the source and the resultant field may be written in terms of a dyadic Green's function given explicitly in the form of (A4) where $\mathbf{f}_i,\mathbf{h}_i$ are the natural vector modes of the system.

APPENDIX B

In this appendix we present the derivation of the dyadic Green's function for the two-plates waveguide, in two different ways. The first is the conventional one, using an eigenfunction expansion method. This approach may be applied to waveguides of different geometries provided the solution to the three-dimensional scalar wave equation is known. The second method, that of the image currents is of limited applicability, but provides a physically meaningful interpretation to the results of Sec. III.

1. Eigenfunction expansion

Here we will only outline the derivation briefly. For more details the reader is referred to the book by Tai.[15] The advantage of Tai's method is that only two sets of vector modes are needed for the expansion. This makes a considerable simplification in solving this type of problem that usually involve a large amount of algebraic manipulations.

The first step is to seek two independent solutions of the homogeneous vector wave equation

$$\nabla\times\nabla\times\mathbf{P}-k^2\mathbf{P}=0 . \tag{B1}$$

Two such solutions are given by

$$\mathbf{M}=\nabla\times(\psi_1\mathbf{u}) , \tag{B2}$$

$$\mathbf{N}=\nabla\times\nabla\times(\psi_2\mathbf{u}) , \tag{B3}$$

where ψ_1, ψ_2 are solutions of the scalar wave equation

$$(\nabla^2+k^2)\psi=0 \tag{B4}$$

and **u** is a constant vector. In a rectangular waveguide the choice of **u** along the axis generates the familiar TE and TM modes. In our case we choose $\mathbf{u}=\hat{\mathbf{y}}$ and the set of solutions

$$\left.\begin{matrix}\psi_o\\ \psi_e\end{matrix}\right\}=\left\{\begin{matrix}\sin\left[\dfrac{m\pi}{b}y\right]\\ \cos\left[\dfrac{m\pi}{b}y\right]\end{matrix}\right\}\times e^{ik_x x+ik_z z} . \tag{B5}$$

The letters e,o stand for even and odd modes with respect to $y=0$. From (B2) and (B3) we obtain

$$\mathbf{M}_o=(-ikz,\ 0\ ,ikx)\sin\left[\frac{m\pi}{b}y\right]e^{ik_x x+ik_z z} , \tag{B6a}$$

$$\mathbf{N}_e=\frac{1}{k}\left[-ik_x\frac{m\pi}{b}\sin\left[\frac{m\pi}{b}y\right],\ k_{\|}^2\cos\left[\frac{m\pi}{b}y\right],\ -ik_z\frac{m\pi}{b}\sin\left[\frac{m\pi}{b}y\right]\right]e^{ik_x x+ik_z z} . \tag{B6b}$$

We note that $\mathbf{M}_o$ and $\mathbf{N}_e$ satisfy the required boundary condition for the electric field.

The matrix equation

$$\nabla\times\nabla\times\overleftrightarrow{G}-k^2\overleftrightarrow{G}=-4\pi\overleftrightarrow{I}\delta(\mathbf{r}-\mathbf{r}') \tag{B7}$$

is now solved. The modes $\mathbf{M}_o, \mathbf{N}_e$ satisfy the appropriate completeness and orthogonality relations and can be used to expand the right-hand side of (B7). Using (B6a) and (B6b) it is then a simple matter to write an expansion for $\overleftrightarrow{G}$. The final result is

$$\overleftrightarrow{G}(\mathbf{r},\mathbf{r}')=\frac{1}{2\pi^2 b}\sum_m \int dk_x \int dk_z \frac{1}{k_{||}^2}\frac{1}{k_{||}^2+\left[\frac{m\pi}{b}\right]^2-k^2}\left[\mathbf{M}_o(\mathbf{r})\mathbf{M}_o^*(\mathbf{r}')-\frac{1}{k^2}\mathbf{N}_e(\mathbf{r})\mathbf{N}_e^*(\mathbf{r}')\right]$$

$$=\frac{1}{2\pi^2 b}\sum_m \int dk_x \int dk_z \frac{1}{k_{||}^2+\left[\frac{m\pi}{b}\right]^2-k^2}\overleftrightarrow{F}(k_x,k_z,m)e^{ik_x(x-x')+ik_z(z-z')}, \tag{B8}$$

where $k_{||}^2=k_x^2+k_z^2$ and the elements of $\overleftrightarrow{F}$ are given by

$$F_{xx}=\left[1-\frac{k_x^2}{k^2}\right]\sin\left[\frac{m\pi}{b}y\right]\sin\left[\frac{m\pi}{b}y'\right],$$

$$F_{yy}=\left[1-\frac{1}{k^2}\left[\frac{m\pi}{b}\right]^2\right]\cos\left[\frac{m\pi}{b}y\right]\cos\left[\frac{m\pi}{b}y'\right],$$

$$F_{zz}=\left[1-\frac{k_z^2}{k^2}\right]\sin\left[\frac{m\pi}{b}y\right]\sin\left[\frac{m\pi}{b}y'\right],$$

$$F_{xy}=-ik_x\frac{m\pi}{b}\frac{1}{k^2}\sin\left[\frac{m\pi}{b}y\right]\cos\left[\frac{m\pi}{b}y'\right],$$

$$F_{yx}=ik_x\frac{m\pi}{b}\frac{1}{k^2}\cos\left[\frac{m\pi}{b}y\right]\sin\left[\frac{m\pi}{b}y'\right],$$

$$F_{zx}=F_{xz}=-\frac{k_xk_z}{k^2}\sin\left[\frac{m\pi}{b}y\right]\sin\left[\frac{m\pi}{b}y'\right],$$

$$F_{yz}=ik_z\frac{m\pi}{b}\frac{1}{k^2}\cos\left[\frac{m\pi}{b}y\right]\sin\left[\frac{m\pi}{b}y'\right],$$

$$F_{zy}=-ik_z\frac{m\pi}{b}\frac{1}{k^2}\sin\left[\frac{m\pi}{b}y\right]\cos\left[\frac{m\pi}{b}y'\right].$$

We note that with the help of the integral representation[18]

$$H_0^{(1)}(k_{||}\rho)=\frac{i}{\pi^2}\int dk_x\int dk_z\frac{e^{ik_x(x-x')+ik_z(z-z')}}{k_{||}^2-k_x^2-k_z^2}$$

$$=\frac{1}{\pi}\int dk_x\frac{e^{ik_x(x-x')+ik_z(z-z')}}{(k_{||}^2-k_x^2)^{1/2}}, \tag{B9}$$

$\overleftrightarrow{G}$ can be put in a more concise form, similar to the Levine-Schwinger solution of the free-space problem

$$\overleftrightarrow{G}=\frac{2\pi i}{b}\sum_m\left[\overleftrightarrow{I}-\frac{1}{k^2}\nabla\nabla'\right]H_0^{(1)}(k_{||}\rho)\times\sin\left[\frac{m\pi}{b}y\right]\sin\left[\frac{m\pi}{b}y'\right]. \tag{B10}$$

2. The image currents method

Consider a charge, moving in the plane $y=y'$ located between the conducting plates, as illustrated in Fig. 8. The electromagnetic field in the region $0\le y\le b$, that satisfies the appropriate boundary conditions on the plates, may be calculated by superimposing the free-space fields of the "image" charges. Those are obtained by multipole reflections of the actual charge with respect to the plates. They have alternating signs and are situated along a line perpendicular to the plates in the planes $y_n=\pm y'+2nb$, $n=0,\pm1,\pm2,\pm3,\ldots$. Using (1.8) the sum of all the free-space fields is given by

$$\mathbf{E}_\omega=ike\int d^3r'\int dt'\left[\overleftrightarrow{I}-\frac{1}{k^2}\nabla\nabla'\right]g_\omega(\mathbf{r},\mathbf{r}')\cdot\mathbf{J}(\mathbf{r}',t'), \tag{B11}$$

where

$$g_\omega(\mathbf{r},\mathbf{r}')=\sum_n\left[\frac{e^{ikR_n^+}}{R_n^+}-\frac{e^{ikR_n^-}}{R_n^-}\right],$$

$$R_n^\pm=[(x-x')^2+(y\mp y'-2nb)^2+(z-z')]^{1/2}.$$

The relation between the description of the field by means of the image construction and the mode analysis discussed earlier, is that of a spatially periodic function and its Fourier transform. To see this, we first represent the spherical waves in (B9) as a combination of plane waves[27]

$$\frac{e^{ikR}}{R}=\frac{i}{2\pi}\int\int\frac{dk_xdk_y}{k_z}e^{ik_x(x-x')+ik_y(y-y')+ik_z(z-z')}\Big|_{k_z=(k^2-k_x^2-k_y^2)^{1/2}}. \tag{B12}$$

We now want to introduce (B12) into (B11) and perform a Fourier transform operation with respect to the y coordinate. Alternatively, one can use the Poisson summation formula[28]

$$\sum_{n=-\infty}^{\infty} f(n)=\sum_{m=-\infty}^{\infty}\left[\int_{-\infty}^{\infty} e^{2\pi i m u} f(u)du\right]. \tag{B.13}$$

Combining Eqs. (B11)—(B13), we obtain

$$g_\omega(\mathbf{r},\mathbf{r}')=\sum_n \frac{i}{2\pi}\int \frac{dk_x dk_y}{k_z} e^{ik_x(x-x')+ik_z(z-z')}\left(e^{ik_y(y-y'+2nb)}-e^{ik_y(y+y'-2nb)}\right)$$

$$=\frac{i}{2\pi}\sum_{m=-\infty}^{\infty}\int \frac{dk_x dk_y}{k_z} e^{ik_x(x-x')+ik_z(z-z')}\left(e^{ik_y(y-y')}-e^{ik_y(y+y')}\right)\int_{-\infty}^{\infty} e^{2\pi i m u-2ik_y bu}du\,. \tag{B14}$$

The last integral on the right-hand side is identified as a δ function

$$\int_{-\infty}^{\infty} e^{2\pi i m u-2ik_y bu}du=\frac{\pi}{b}\delta\left[k_y-\frac{m\pi}{b}\right]. \tag{B15}$$

Inserting (B15) into (B14) and making the sum over positive integers only yields

$$g_\omega(\mathbf{r},\mathbf{r}')=\frac{2i}{b}\sum_{m>0}\int \frac{dk_x}{k_z} e^{ik_x(x-x')+ik_z(z-z')}\sin\left[\frac{m\pi}{b}y\right]\sin\left[\frac{m\pi}{b}y'\right]. \tag{B16}$$

Finally, using the last part of (B9) [which is in fact a plane-wave representation in two dimensions analogous to (B12)], we get

$$g_\omega(\mathbf{r},\mathbf{r}')=\frac{2\pi i}{b}\sum_{m=1}^{\infty} H_0^{(1)}(k_{||}\rho)\sin\left[\frac{m\pi}{b}y\right]\sin\left[\frac{m\pi}{b}y'\right] \tag{B17}$$

as desired.

---

*Present address: Università degli Studi di Lecce, via Arnesano, I-73100 Lecce, Italy.

[1]H. Motz, J. Appl. Phys. **22**, 527 (1951).
[2]B. Kincaid, J. Appl. Phys. **48**, 2684 (1977).
[3]W. B. Colson, Ph. D. dissertation, Stanford University, 1977.
[4]W. B. Colson, IEEE J. Quantum Electron. **QE-17**, 1417 (1981).
[5]P. Bosco and W. B. Colson, Phys. Rev. A **28**, 319 (1983).
[6]C. Bazin *et al.*, in *Free-Electron Generators of Coherent Radiation,* in Vol. 8 of *Physics of Quantum Electronics* (Addison-Wesley, New York, 1982).
[7]W. B. Colson, G. Dattoli, and F. Ciocci, Phys. Rev. A **30**, 828 (1985).
[8]D. A. G. Deacon *et al.,* Phys. Rev. Lett. **38**, 892 (1976); Proc. SPIE **121**, 89 (1977).
[9]J. D. Jackson, *Classical Electrodynamics* (Wiley, New York, 1975).
[10]L. R. Elias and J. C. Gallardo, Appl. Phys. B **31**, 229 (1983).
[11]L. R. Elias and G. J. Ramian, in *Free-Electron Generators of Coherent Radiation,* edited by C. H. Brau [Proc. SPIE **453**, 137 (1983)].
[12]A. Amir *et al., IEEE 8th Conference on Infra-Red and Millimeter Waves, Miami Beach, Florida, 1983* (Institute of Electrical and Electronic Engineers, New York, 1983).
[13]H. Motz and M. Nakamura, Ann. Phys. **7**, 84 (1959).
[14]H. A. Haus and N. Islam, J. Appl. Phys. **54**, 9 (1983).
[15]C. T. Tai, *Dyadic Green's Functions in Electrodynamic Theory* (Intext Educational Publishers, Scranton, 1971).
[16]J. M. J. Madey, Nuovo Cimento B **50**, 64 (1979).
[17]C. H. Chen, *Theory of Electromagnetic Waves—A Coordinate-Free Approach* (McGraw-Hill, New York, 1983).
[18]P. M. Morse and H. Feshbach, *Methods of Theoretical Physics* (McGraw-Hill, New York, 1953), Vol. I, p. 811.
[19]M. Born and E. Wolf, *Principles of Optics,* 6th ed. (Pergamon, New York, 1980).
[20]H. Levine and J. Schwinger, Commun. Pure Appl. Math. **3**, 355 (1950).
[21]L. Elias, J. Gallardo, and D. Gregoire (unpublished).
[22]A. Yariv, *Quantum Electronics* (Wiley, New York, 1975).
[23]A. Amir, Quantum Institute (University of California, Santa Barbara) Internal Report, QI-FEL-033/84 (unpublished).
[24]M. Lax *et al.,* Phys. Rev. A **11**, 1365 (1975).
[25]W. B. Colson and P. Elleaume, Appl. Phys. **29**, 101 (1982).
[26]A. Amir and L. Elias, in *Lasers in Fluid Mechanics and Plasmadynamics, AIAA 16th Conference,* edited by C. P. Wang (American Institute of Aeronautics and Astronautics, New York, 1983).
[27]A. Banos, *Dipole Radiation in the Presence of a Conducting Half-Space* (Pergamon, New York, 1970), p. 18.
[28]M. Spiegel, *Mathematical Handbook* (McGraw-Hill, New York, 1970).